

RESEARCH PAPER

Solvent-Free Hydrothermal Synthesis of Network-Like Graphene Quantum Dots (GQD) Nano Particle and Ultrasonic TiO₂/GQD Nanocomposite

Mohammed Thamer Jaafar¹, Luma Majeed Ahmed^{2*}, Rahman Tama Haiwal²

¹ Department of Petroleum Engineering, College of Engineering, University of Kerbala, Karbala, Iraq

² Department of Chemistry, College of Science, University of Kerbala, Karbala, Iraq

ARTICLE INFO

Article History:

Received 04 March 2023

Accepted 13 June 2023

Published 01 July 2023

Keywords:

Amides Derivative

Amin Derivatives

GQD

Hydrothermal

Porphyrin Derivatives

Solar Cells

ABSTRACT

The enhancement of solar cell efficiency, is required to use materials of a good electrical properties. In this work, the graphene quantum dots (GQD) created from starch as precursor has been performed in single pot using a hydrothermal process. The TiO₂/GQD nanocomposite was prepared using an in-depth ultrasonic technique to use as a semiconductor in a solar cell. The investigated using techniques such as: FT-IR, FE-SEM, XRD, Raman spectrum. Additionally, the synthesis and the characterization of novel porphyrin derivatives with amide, were designed as sensitizers in dye-synthesized solar cells (DSSCs). Five derivatives were synthesized via a one-pot reaction of porphyrin with amines, and their optimal yield was obtained under various conditions. The synthesized dyes were characterized using techniques such as melting point analysis, mass spectroscopy, FT-IR, ¹H, ¹³C-NMR and ESI-Mass. The obtained results demonstrated that the 6b dye exhibited with the high efficiency of 1.86 % at AM 1.5, followed by 6a with 1.82 %, 8a with 1.34 %, and 8b with 1.14 %, as compared to the control cell (N719) with an efficiency of 5.4 %.

How to cite this article

Jaafar M. T., Ahmed L. M., Haiwal R. T. Solvent-Free Hydrothermal Synthesis of Network-Like Graphene Quantum Dots (GQD) Nano Particle and Ultrasonic TiO₂-GQD Nanocomposite. J Nanostruct, 2023; 13(3):626-638. DOI: 10.22052/JNS.2023.03.003

INTRODUCTION

Graphene quantum dots (GQDs) are a novel class of carbon materials that have drawn a lot of interest for their tunnelable PL characteristics, low toxicity, hydrophilic makeup, favorable biocompatibility, and superior photo-stability [1-5]. Graphene quantum dots (GQDs), a kind of carbon-based quantum dot, have lately been employed in DSSC applications because of its high PL quantum yield, chemical stability, low toxicity, and very high optical absorptivity [6, 7]. One or more graphene layers having a thickness of 20

nm or less are referred to as zero-dimensional (0 D) GQDs. Due to their quantum size and edge effects, GQDs have a bandgap that is less than 2.0 eV [8]. Due to the fact that the bandgap of GQDs changes with their size, replacing ruthenium-based dye with them as a green photo-sensitizer is thought to be a novel strategy for greater efficiency DSSCs. Reduced GQD size, according to Li and Hu [9], not only allows for more effective bandgap adjustment but also makes a broad range of applications possible. The first functional DSSCs were created in 1991 by O'Regan and colleagues,

* Corresponding Author Email: luma.ahmed@uokerbala.edu.iq



with a power conversion efficiency (PCE) of 7% when illuminated by AM 1.5 [10]. Ten years later, TiO₂ nano powder was used as a semiconductor electrode by Naseeruddin and colleagues, and the efficiency of DSSCs was reported to be 11.4 percent [11, 12]. For DSSCs, a large selection of organic dyes with the donor and acceptor system have been developed [13-15]. According to earlier research, modifying photoelectrodes with a combination of GQD and TiO₂ may increase DSSC efficiency. In order to help dye-Sensitized TiO₂-PA, Xiaoli Fang and his colleagues produced GQDs. They looked at how the GQDs affected the DSSCs' and TiO₂ photoanode's characteristics. According to Kim and Lee [16, 17], using GQD (about 5.0–10.0 nm) TiO₂ layers enhanced the performance of DSSCs. In our earlier study, we successfully created GQDs using the hydrothermal method, and we looked into the functionality of DSSCs that used ZnO photo-anodes (ZnO) by replacing N-719 with GQDs as a photo-sensitizer. The GQDs may be used as an alternative to ruthenium-based dyes as the efficiency of DSSC employing ZnO submerged in GQDs is comparable to devices using N-719 [18]. To boost the PCE of DSSCs, the photo-anode is crucial. The impact of immersion duration and photoanode thickness must be studied in order to increase the efficiency of DSSCs that use GQDs as the photosensitizer. Porphyrins are often excellent candidates for use as the primary ingredient in photocatalytic catalysts [19]. The porphyrins have a wide visual absorption spectrum at a high molecular absorption coefficient due to the massive delocalized π -electron system [20]. Porphyrins are also widely distributed in nature, easy to synthesize, and photochemically stable. By adjusting the substituents and central metal species, several investigations have been conducted to investigate the uses of porphyrins. For example, the correlations between the dye structure and solar cell efficiency [21], the interfacial charge transfer mechanism [22], and photocatalysis performance [23] have been the subject of several landmark results in the porphyrin research field [24].

This work focused on the synthesis of graphene quantum dot (GQD) using solvent free hydrothermal method from starch as precursor, and incorporated it with TiO₂ as a nanocomposite by ultrasonic technique. The synthesis of new amides from porphyrin derivatives as four compounds will prepared with amines derivatives.

The characterization of all prepared compounds will do and then test them as solar cells where the one of the electrodes which is TiO₂/GQD, and other electrode is gold.

MATERIALS AND METHODS

Preparation of Graphene Quantum Dot GQD

The starch was used as the green precursor in the quick and simple hydrothermal process that produced the GQDs. The chemical mechanism is explained, showing that the synthetic process includes both the initial hydrolysis of starch to create glucose and the subsequent ring-closure condensation of glucose to make GQDs. Because of the comparatively large levels of the ionic product of H⁺ and OH under hydrothermal conditions, water is first employed as a hydrolytic medium. The starch will then constantly hydrolyze with water and no chemical agent in the presence of H⁺ to produce a variety of components, such as glucose, fructose, maltose, and aldehydes. According to the carbon balances, traces of gaseous products are also created, albeit they are comparatively minor. As the hydrolysis process progresses, the output of glucose rises while that of other carbohydrates drastically declines. As a result, the starch is mostly transformed into glucose, with trace quantities of other carbs remaining. Accordingly, in hydrothermal circumstances, dehydration occurs via interactions between hydrogen atoms of one glucose molecule and the hydroxyl groups of an adjacent glucose molecule as well as from reactions between formyl groups and hydroxyl groups. As a result, carbon atoms engage in covalent interactions with one another to create aromatic rings, the fundamental building block of the graphene structure. In this manner, the ring-closure condensation of glucose molecules results in the formation of GQDs. On the other hand, the carbonization process converts the remaining carbohydrates into carbide precipitates at high temperatures and pressures. Generally, the GQDs solution is produced by filtering the precipitates away (Fig. 1) [3].

Preparation of TiO₂/GQD nanocomposite

The GQD modified by TiO₂ using indirect ultrasonic method. 1 g of TiO₂ was dispersive in 50 mL of ethanol in a beaker, using an ultrasonic for 1h. In other baker, 0.1g from the GQD was dispersive in the 5 mL of ethanol using ultrasonic bath also for 1h. The GQDs and TiO₂ nanoparticles

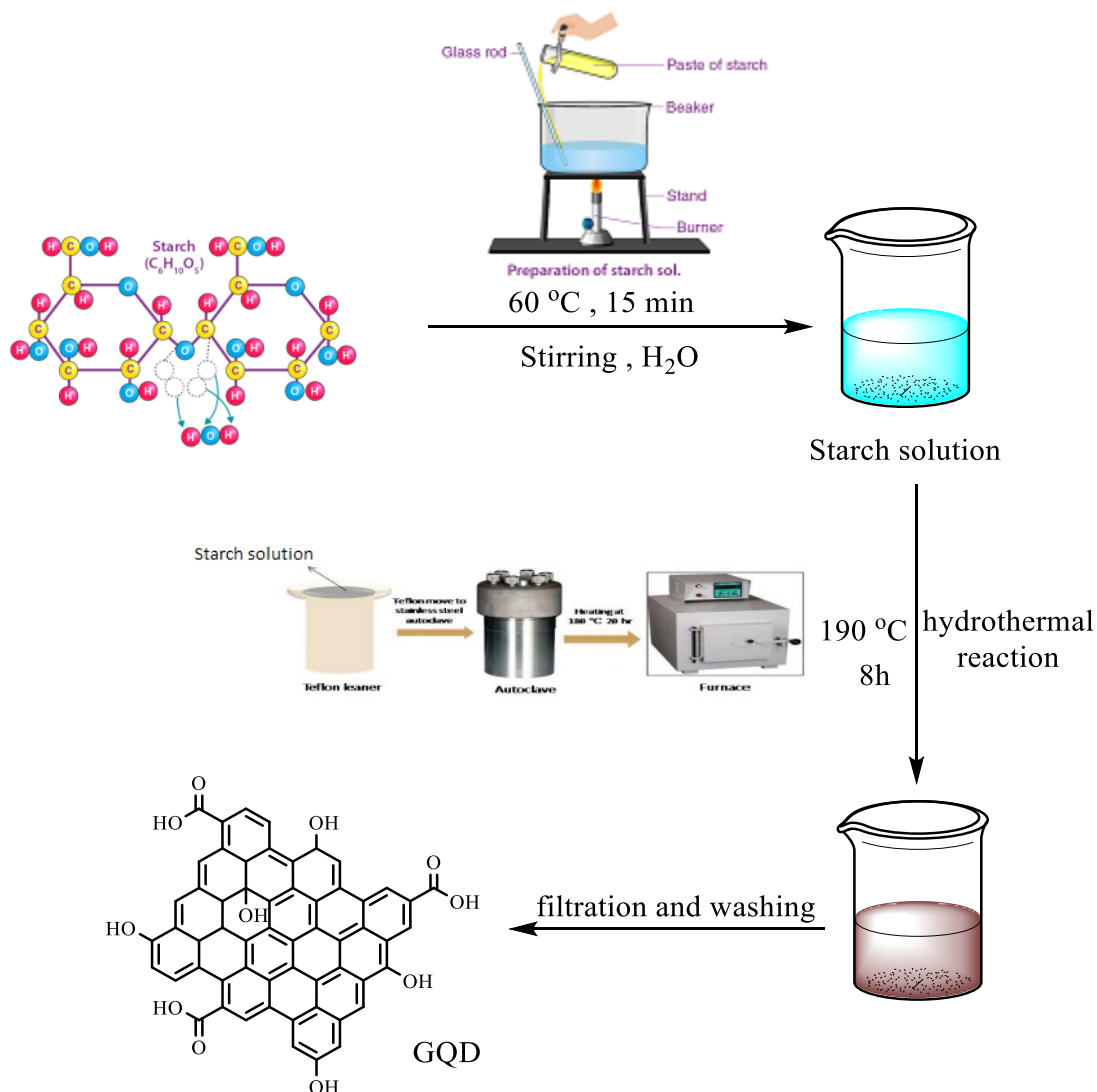


Fig. 1. The green method of synthesis for GQDs.

were linked together as nano-composite depended on the ultrasonic energy that enhanced their interaction and bonding.

Synthesis porphyrin derivatives

Material and instruments of porphyrin derivatives

The chemicals used in this study were purchased from a number of manufacturers, such as Sigma Aldrich, and were used directly in this work without any further purification. On a digital Electro-Thermal Stuart SMP-30, melting points were measured and found to be accurate. Fourier transform infrared spectroscopy (SHIMADZU FTIR-8400S) and were expressed in cm⁻¹. Nuclear magnetic resonance spectra were performed in

DMSO-d₆ on a Bruker spectrometer (500 MHz for ¹H NMR, 125 MHz for ¹³C NMR). ESI-mass spectra were obtained on an Agilent Technology (HP) instrument (EI, 70 eV).

Synthesis of 4-(10,15,20-tris(3-hydroxyphenyl) porphyrin-5-yl) benzoic acid (4)

pyrrole (4 mol) was added to a solution of substituted aldehyde (4-formylbenzoic acid) (1 mol) and (3-hydroxy benzaldehyde) (3mol) in propionic acid (20 mL), and the reaction mixture was refluxed for one hour in the dark after that. After that, the solution was filtered and washed with water hot.

4-(10,15,20-tris(3-hydroxyphenyl) porphyrin-5-yl)

benzoic acid (4)

Color: Black powder: Yield 25%, mp > 350°C FT-IR (KBr, Cm⁻¹):3309-2400(OH), 3009(C-H aromatic), 1708(C=O), 1585 (C=N), 1485(C=C), 1222(NH band), ¹HNMR (500MHz, DMSO-d₆): δH (ppm): 12.49 (s,1H-COOH). 8.83-8.41 (m,8 Pyrrole-H), 8.11-7.29 (m 13 Ar-H), 7.06 (s, 3OH), 6.76 (m, 3H), -1.45 (s,1NH_{int}), -2.64 (s,1NH_{int}), ¹³C NMR (500MHz, DMSO-d₆) δ C 115.59, 120.25, 120.28, 122.22, 122.52, 123.76, 123.89, 123.99, 126.57, 126.64, 129.64, 126.99, 127.06, 128.55, 128.94, 129.60, 129.67, 130.56, 130.64, 136.36,136.52, 139.86, 143.44, 143.88, 146.84, 153.68, 153.68, 156.14, 169.36., EI-MS calcd exact mass (C₁₀₃H₆₇N₁₁O₈) 706.76; found, 706.6.

Prepare Compound 6a,6b

1 mmol of SOCl₂ was added of (2 mmol) 4-(10,15,20-tris(3-hydroxyphenyl) porphyrin-5-yl) benzoic acid. The mixture was stirred at 70 rpm for 30 minutes at environmental temperature, then DMF (5mL) was added with continuous stirred for 10 minutes at same temperature. The final solution was transferred to round bottom flask volume (25 mL), amines (benzidine, 4,4'-Oxydianiline) were added to the last solution with reflux at 120 °C for 2 hours, and then triethylamine (Et₃N) was added with continuous reflux at 120 °C for 1huore. The black solution was added to ice crystal, filtration and washing by ethanol.

N, N'-([1,1'-biphenyl]-4,4'-diyl) bis(4-(10,15,20-tris(3-hydroxyphenyl) porphyrin-5-yl) benza-mide) (6-a)

Color: Black powder: Yield 65%, mp > 350°C FT-IR (KBr, Cm⁻¹):3406(NH Stretch), 3200-2400(OH), 3051(C-H aromatic), 1697(C=O), 1600 (C=N), 1508 (C=C), ¹HNMR (500MHz, DMSO-d₆): δH (ppm): 9.61 (s,2H-CONH). 8.80-814 (m,16 Pyrrole-H)), 8.06-7.17 (m 34 Ar-H), 7.05 (s, 6OH), 6.86 (m, 6H), -1.45 (s,2NH_{int}), -1.74 (s,2NH_{int}),. ESI-MS calcd exact mass (C₁₀₂H₆₈N₁₀O₈), 1561.73; found, 1561.69.

N,N'-(oxybis(4,1-phenylene)) bis(4-(10,15,20-tris(3-hydroxyphenyl) porphyrin-5-yl) benzam-ide) (6-b)

Color: Black powder: Yield 65%, mp > 350°C FT-IR (KBr, Cm⁻¹):3414(NH Stretch), 3200-2400(OH), 3051(C-H aromatic), 1693(C=O), 1581 (C=N), 1442(C=C), 578(C-O), ¹HNMR (500MHz,

DMSO-d₆): δH (ppm): 9.90 (s,2H-CONH), 8.88-8.27 (m,16 Pyrrole-H)), 8.13-7.11 (m 34 Ar-H), 7.09 (s, 6OH), 6.61 (m, 6H), -1.43 (s,2NH_{int}), -1.61 (s,2NH_{int}),. EI-MS calcd exact mass (C₁₀₂H₆₈N₁₀O₉), 1577.73; found, 1577.69.

Prepare Compound 8a,8b

1 mmol of SOCl₂ was added of (1 mmol) 4-(10,15,20-tris(3-hydroxyphenyl) porphyrin-5-yl) benzoic acid. The mixture was stirred at 70 rpm for 30 minutes at environmental temperature, then DMF (5mL) was added with continuous stirred for 10 minutes at same temperature. The final solution was transferred to round bottom flask volume (25 mL), amines (2-amino Benzimidazole, 1-(4-amino phenyl) ethan-1-one) were added to the last solution with reflux at 120 °C for 2 hours, and then triethylamine (Et₃N) was added with continuous reflux at 120 °C for 1huore. The black solution was added to ice crystal, filtration and washing by ethanol.

N-(1H-benzo[d]imidazol-2-yl)-4-(10,15,20-tris(3-hydroxyphenyl) porphyrin-5-yl)benzamide (8-a)

Color: Black powder: Yield 66%, mp > 350°C FT-IR (KBr, Cm⁻¹):3410(NH Stretch), 3248-2400(OH), 3066(C-H aromatic), 1697(C=O), 1600 (C=N), 1481(C=C), ¹HNMR (500MHz, DMSO-d₆): δH (ppm): 11.37(s, 1NH), 10.43 (s,1H-CONH). 8.45 (m,8 Pyrrole-H)), 8.11-7.18 (m 17 Ar-H), 7.06 (s, 3OH), 6.90 (d, J = 2.2 Hz, 3H), -1.45 (s,1NH_{int}), -2.64 (s,1NH_{int}),. ¹³C NMR (500 MHz, DMSO-d₆) δ C 94.40, 100.01, 115.66, 123.03, 126.94, 129.82, 130.04, 130.43, 130.57, 138.63,144.17,144.77, 147.97, 156.63, 156.83, 162.84, 163.35, 167.30, 168.90., Anal. Calcd for (C₅₂H₃₅N₇O₄): C, 75.99; H, 4.29; N, 11.93; O, 7.79 found C, 75.85; H, 4.20; N, 11.74%.,

N-(4-acetylphenyl)-4-(10,15,20-tris(3-hydroxyphenyl) porphyrin-5-yl) benzamide (8-b)

Color: Black powder: Yield 60%, mp > 350°C FT-IR (KBr, Cm⁻¹):3302(NH Stretch), 3228-2400(OH), 3016(C-H aromatic), 2928 (C-H aliphatic), 1697(C=O), 1597 (C=N), 1481(C=C),. ¹HNMR (500MHz, DMSO-d₆): δH (ppm): 9.26 (s,1H-CONH). 8.52-8.36 (m,8 Pyrrole-H)), 8.14-7.20 (m 17 Ar-H), 7.02 (s, 3OH), 6.84 (d, J = 2.2 Hz, 3H), 3.64 (s, 3 CH₃), -1.45 (s,1NH_{int}), -2.64 (s,1NH_{int}),. ¹³C NMR (500 MHz, DMSO-d₆) δ C 94.40, 100.01, 115.66, 123.03, 126.94, 129.82, 130.04, 130.43, 130.57, 138.63, 144.17, 144.77, 147.97, 156.63, 156.83, 162.84, 163.35, 167.30, 168.90., Anal. Calcd for



(C₅₃H₃₇N₅O₅): C, 77.26; H, 4.53; N, 8.50; O, 9.71 found C, 77.16; H, 4.42; N, 8.35%.

Preparation and testing DSSCs

Fluorine-doped Tin Oxide (FTO) glass sheet were cleaned using an ultrasonic bath and washed with distilled water and ethanol. 3.0 g of TiO₂/GQD nano powder were combined with 15 mL of ethanol, 2.5 mL of Triton X-100, and stirred TiO₂/GQD. To create TiO₂/GQD paste, the mixture was agitated under moved using a tiny magnetic bar for 45 minutes. Using an eye dropper, the TiO₂/GQD paste was put onto the FTO glass sheet, where it was then applied using the doctor blade

method to create a thin coating of TiO₂/GQD (0.5 cm² area). The glass sheet with the TiO₂/GQD layer was heated for 30 minutes at 70 °C before being sintered for 45 minutes at 400 °C. The deposit TiO₂/GQD was submerged in the dye solution (10⁻³ mL) for 5 hours after cooling. A gold was used to draw the counter electrode on a piece of another conducting glass (FTO). By sandwiching the TiO₂/GQD thin layer with dye and counter electrode with an I⁻/I³⁻ redox electrolyte solution, a DSSC was created.

Fabricated solar cells were tested using a solar simulator equipped with a 450 W xenon light source (Osram XBO 450) and filter (Schott 113) for DSSCs.

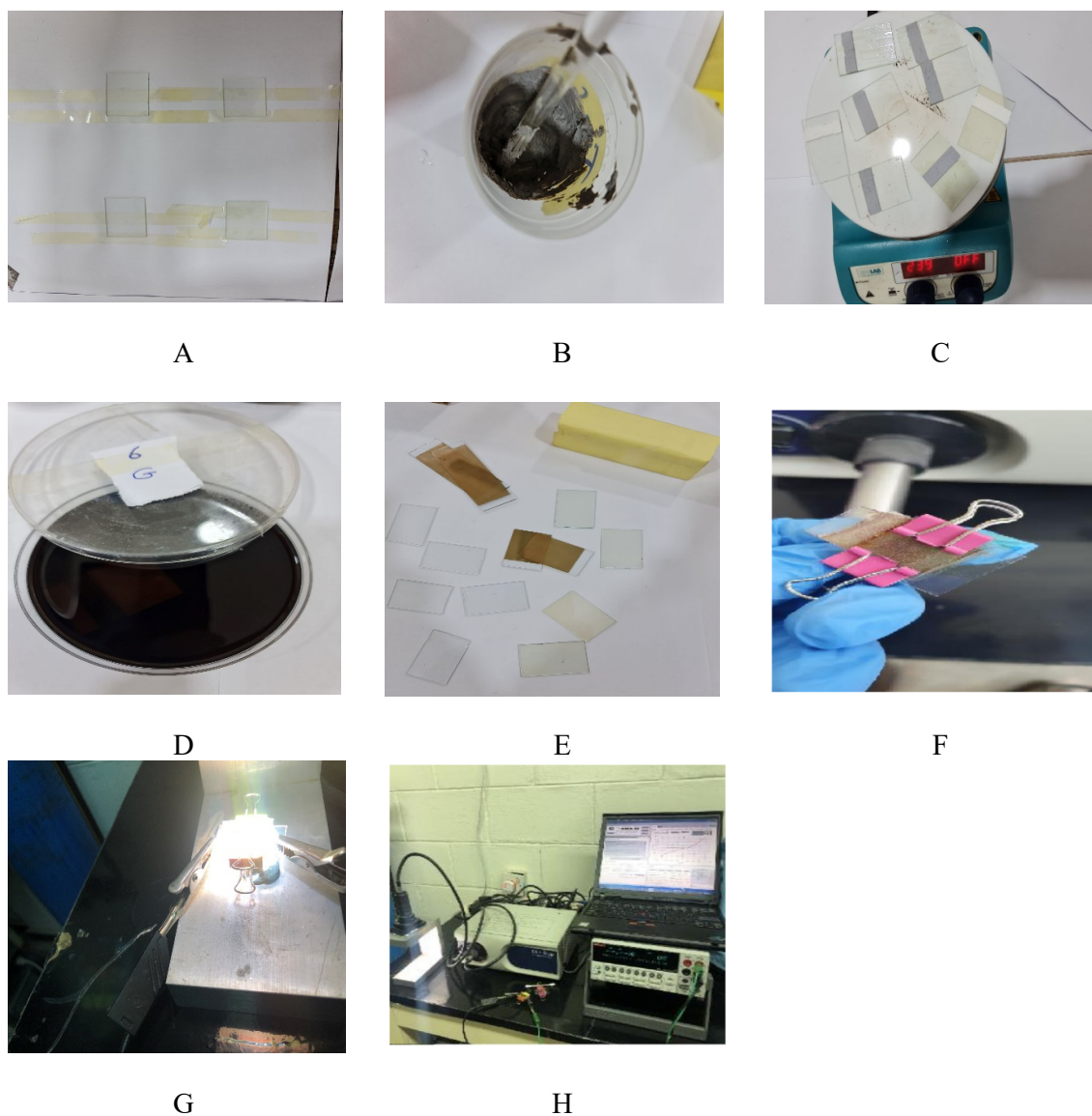


Fig. 2. Steps of Fabrication DSSCs.

By employing a Si photodiode was employed as a reference, along with a KG⁻³ Schott color-matched filter, to minimize the mismatch in wavelength (350-750) nm between AM 1.5 and simulated light to less than 5%. The power of the solar simulator was regulated to the standard test of the DSSCs AM 1.5. To perform JV characterization of the solar cells, a digital source meter (Keithley model 2400) was used to establish an 80 ms delay between voltage and current density.

Preparation of the Counter Electrode (CE)

A drop of iodine solution between two prepared electrodes was added. An iodine solution was prepared by combining (0.05M) of iodine(I₂) with (0.5M) of potassium iodide (KI) in solvent of ethylene glycol and acetonitrile with a volume ratio of (4:1), respectively. The solution is then maintained in an opaque container after shaking the flask until the iodine has fully dissolved. In order to prevent the solution from leaking beyond of the designated cell region, the counter electrode is then put on the working electrode and the solution is retained in an opaque container.

Fig. 2 illustrates the steps involved in the

fabrication of dye-sensitized solar cells (DSSCs): (A) starting with a cleaned FTO substrate was install it, (B) prepared of the anode part of cells were performed by a mixture of TiO₂/GQD nanoparticles, ethanol, and Triton X-100 as a paste, (C) the TiO₂/GQD layer is annealed via heating by heater, (D) the FTO substrate with the TiO₂/GQD layer is immersed in a dye solution, (E) a gold electrode is put onto the dye-coated substrate to be contacted, (F) the DSSC structure is completed, (G) the power output of the solar cell is applied, (H) a source meter (Keithley model 2400) is used for measured the active signal.

RESULTS AND DISCUSSION

Synthesis of Compounds 4, (6a, b), (8a, b)

The first step included the preparation of a compound (4) by the reaction of pyrrole (1) with 4-formylbenzoic acid (2) and 3-hydroxybenzaldehyde in the presence of propanoic acid as a catalyst and a solvent at the same time (Fig. 3). This product was diagnosed using the infrared spectrum by the appearance of OH, and CO groups in carboxylic acid at radii of 3309, and 1708 cm⁻¹, respectively. The ¹H-NMR

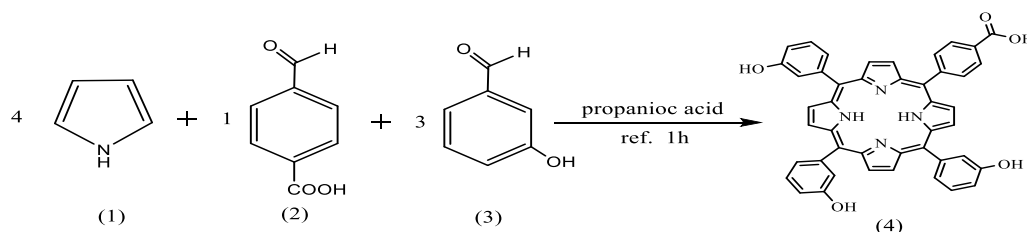


Fig. 3. preparation of compound 4.

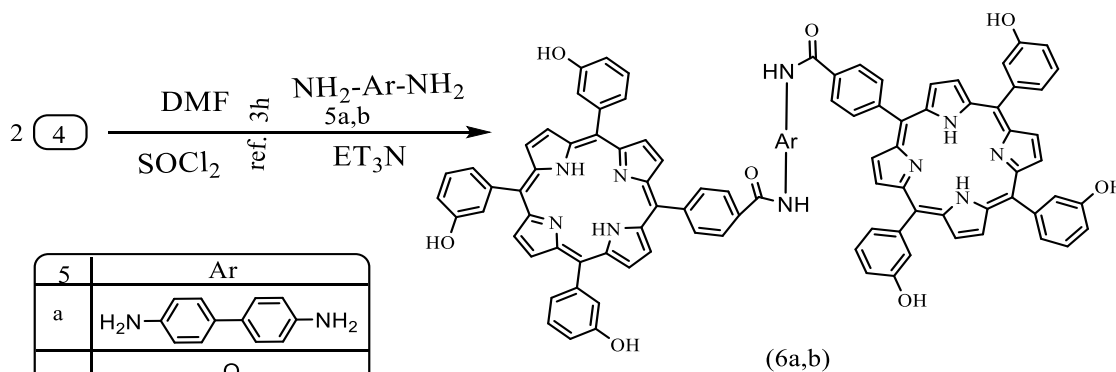


Fig. 4. Preparation of compound (6a, b).

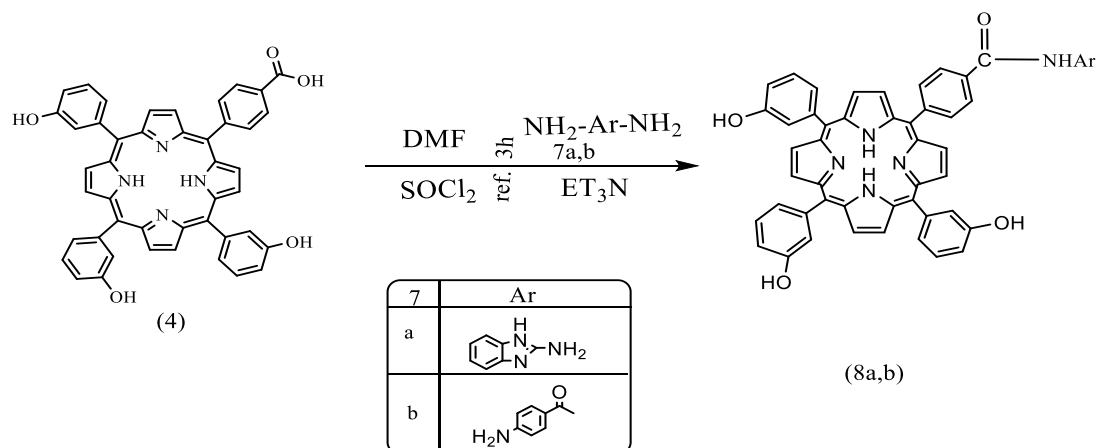


Fig. 5. Preparation of compound (8a, b).

spectra of compound 4 showed a singlet signal at -1.45(1H), -2.64 (2H), which can be attributed to the N-H in the pyrrole group and singlet signal at 12.49 (1H) which can be attributed to the COO-H in the benzoic acid.

The second step involved the reaction of compound (4) with a variety of amines to obtain (6a-b) and (8a, b), as explained in (Fig. 4 and Fig. 5). These compounds were investigated using infrared spectrum by disappearing the carbonyl group and appearing the amide group. The Experimental part provides all of the porphyrin derivatives' complete spectrum information (ESI-MS, FT-IR, ¹H, and ¹³C NMR), as well as melting points. Compound (4) was reacted with a variety of amines in the second step to produce compound (6a-c) and (8a, b), as displayed in (Fig. 4 and Fig. 5). Using an ¹H NMR, these compounds were identified by

the disappearance of the OH in carboxylic acid (12.49) and the appearance of the amide group about (10.40-9.60). The Experimental section gives comprehensive spectral data (MS, FT-IR, ¹H, and ¹³C NMR) and melting points for all porphyrin derivatives.

Characterization of graphene quantum dots

The graphene quantum dots nanoparticle were prepared in one-pot of compounds (6a, b), (8a, b). Particularly, the graphene quantum dots nanoparticle were studied by FE-SEM, FT-IR, Raman, and XRD analyses. In instance, Fig. 6 depicted the nanoparticle shape of graphene quantum dots. The FE-SEM picture revealed the flat and network-like sheets of nanoparticle graphene quantum dots. In Fig. 6 that the graphene quantum dots nanoparticle are made

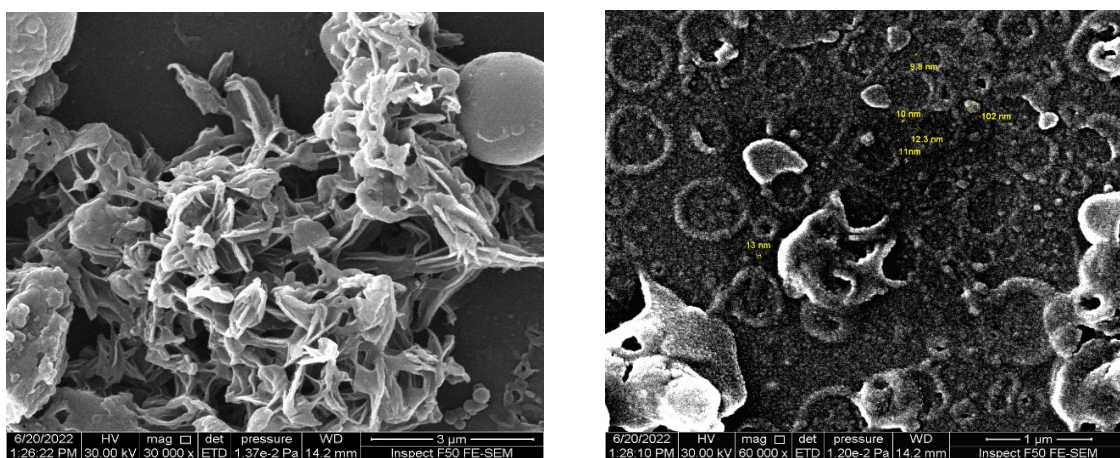
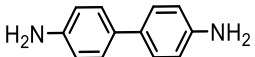
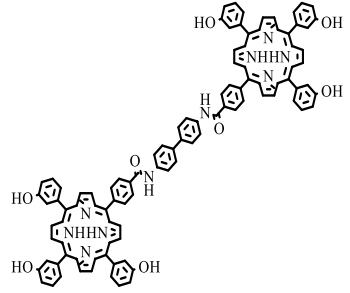
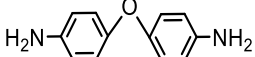
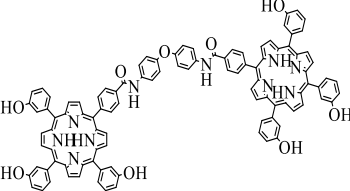
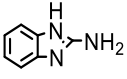
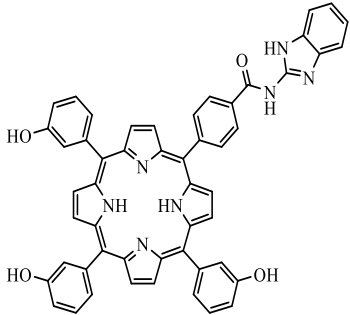
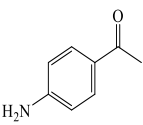
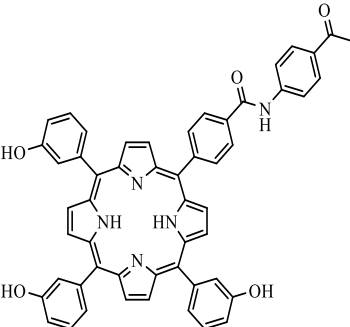


Fig. 6. FE-SEM image of GQD.

Table1. Some of the physical characteristics and mass data of synthetic dyes.

Entry	Amine	Product	Molecular formula	M. Wt. (g/mol)	Yield	Mass Data (m/z) [M+]
6a			C ₁₀₂ H ₆₈ N ₁₀ O ₈	1561.73	65	1561.69
6b			C ₁₀₂ H ₆₈ N ₁₀ O ₉	1577.73	65	1577.69
8a			C ₅₂ H ₃₅ N ₇ O ₄	821.90	66	820.52
8b			C ₅₃ H ₃₇ N ₅ O ₅	823.91	60	822.30

of aggregated and crumpled thin sheets, which are also visible with folds and wrinkles on their surface.

The FT-IR spectrum of the graphene quantum dots nanoparticulate was shown in Fig. 7. The peak

at about 1516 cm⁻¹ is attributed to carbon-carbon double bonds in the sheets of graphene quantum dots. Moreover, other peaks at 3394, 2970, 1701, and 1041 cm⁻¹ could be assigned to hydrogen-oxygen, carbon-hydrogen, carbonyl, and carbon-

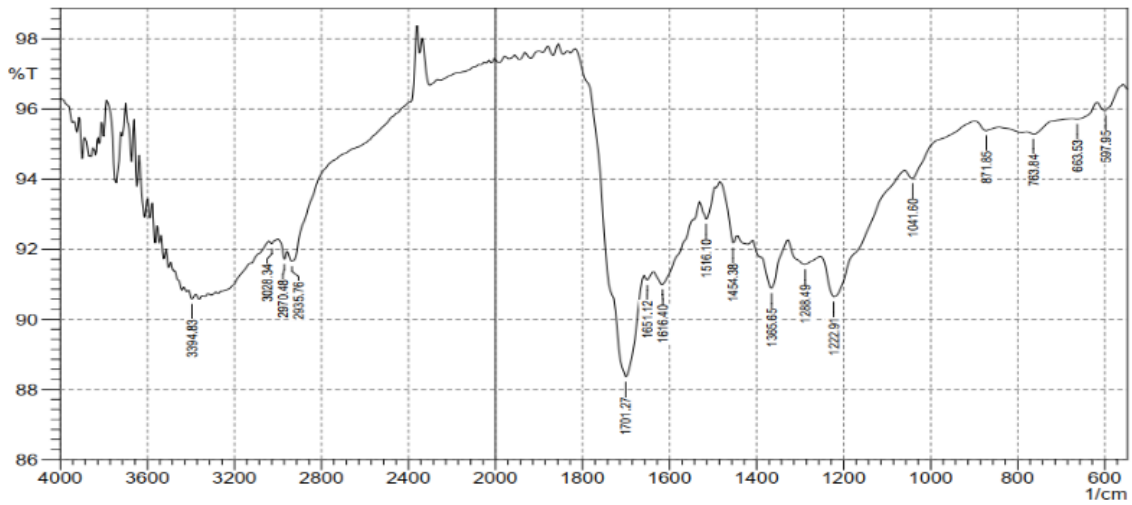


Fig. 7. FT-IR spectrum of GQD.

oxygen stretching modes of functional groups such as carboxylic and hydroxyl groups attached to graphene quantum dots, respectively.

In order to describe the graphene structure of the generated GQDs, Raman spectroscopy was also used. As shown in Fig. 8, two Raman peaks for the GQDs may be attributed to well-ordered graphite (G-band) and disordered sp² carbon, respectively, at around 1352 and 1567 cm⁻¹ in the Raman spectrum. The fact that the G-band is more intense than the D-band suggests that the GQDs contain fewer lattice flaws[3]. Because of the ratio

D peak to G peak is less one that enhancement the amorphous and nanostructure of GQD.

Fig. 9 shows the results of the XRD analysis of the synthesized GQD's structure using a Lab X XRD 6000-Shimadzu. The three crucial not-sharp peaks were seen in the XRD data of the GQD-synthesized powder, with diffraction patterns at 2θ = 28.03°, 12.38°, and 21.92°. Using Scherer's equation (1) [25-30].

$$L = \frac{K \cdot \lambda}{\beta \cdot \cos\theta} \quad (1)$$

L represents the average size of the crystal,

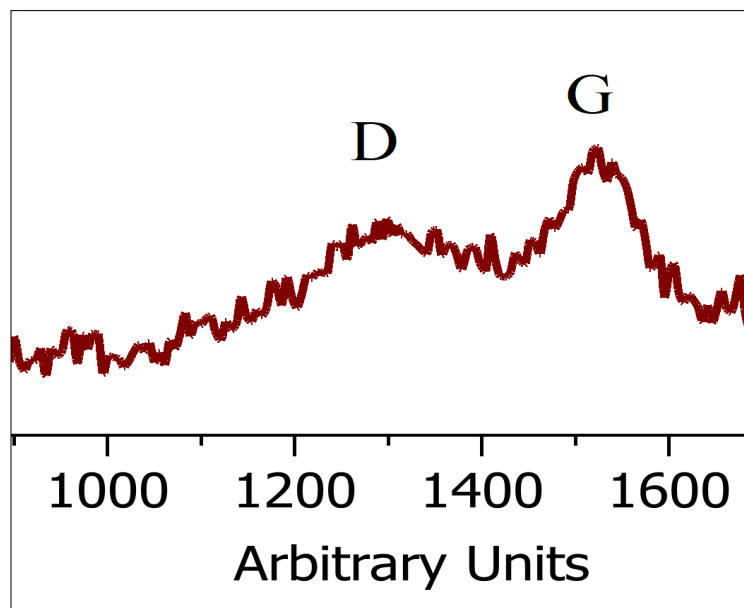


Fig. 8. Raman spectrum of GQD.

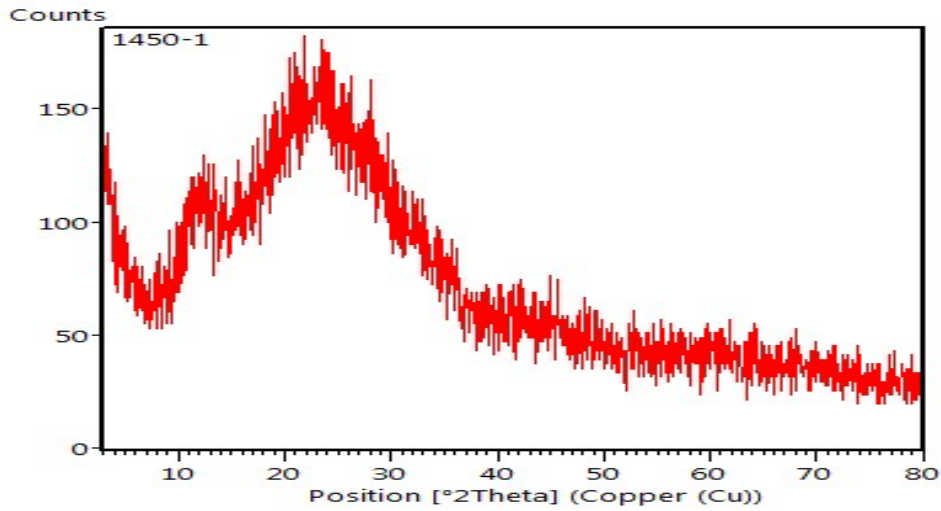


Fig. 9. XRD analysis of GQD.

and it is calculated using the equation (1). The value of k , which is a Scherrer's constant that depends on the shape of the crystal, is set to 0.9[31-33]. The wavelength of the X-ray radiation used for measurement is denoted by λ , which is 0.15406 nm for $\text{Cu}_{\text{K}\alpha}$. The full width of the half-maximum (FWHM) intensity expressed in radians is represented by β (originally in degrees, β is converted to radians by multiplying it by $\pi/180$). The diffraction (Bragg) angle is denoted by θ .

The mean crystallite size (L) in nm for graphene quantum dots nanoparticular was found to be 9.25

nm. The size is ensuring the generated graphene is really quantum dots seems to be nanoscale (less than 10 nm)[34-37].

Characterization of TiO₂/GQD nanocomposite

The FT-IR spectrum of the composite TiO₂/GQD nanoparticular was shown in (Fig. 10). The prepared composites with broad absorption bands at 3000-3600 cm^{-1} are attributed to the OH stretching vibrational absorptions bond. This suggests that there are numerous hydroxyl groups present on the surface of the TiO₂/GQD. The

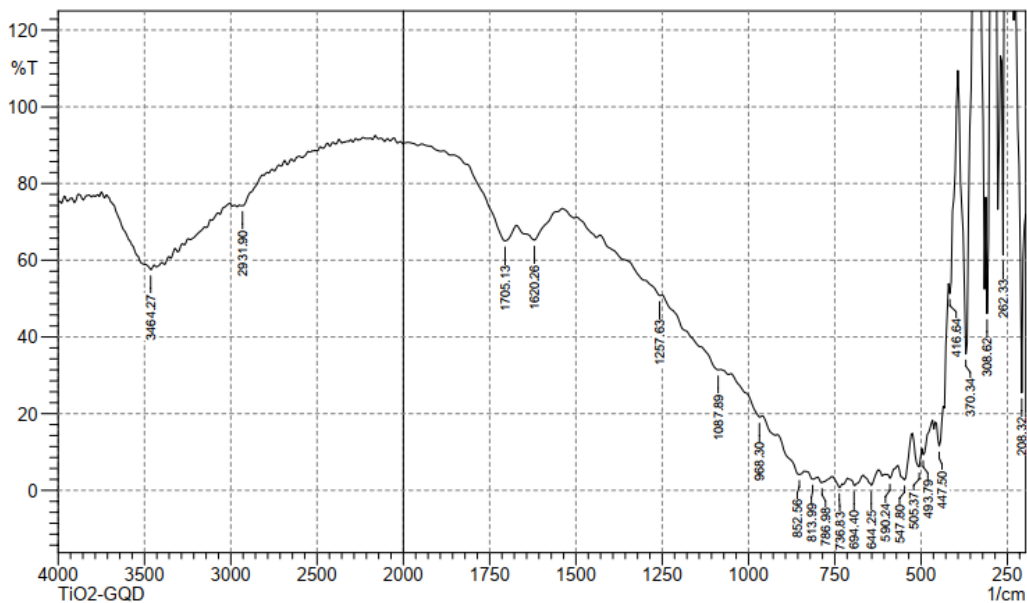


Fig. 10. FT-IR spectrum of TiO₂/GQD.

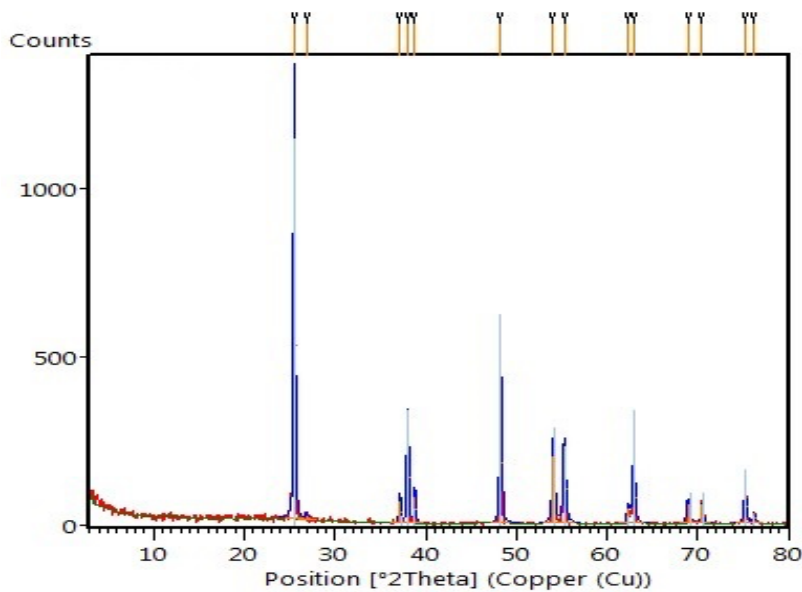


Fig. 11. XRD analysis of GQD/TiO₂.

strong intensity peak at 1705 cm⁻¹ is associated with the C=O stretching vibration in COOH. The edge of board peaks in TiO₂ ranged from 675 to 426 cm⁻¹ shifts toward high frequency from 477 to 852 cm⁻¹ after incorporated to formed a TiO₂/GQD composite. These spectra prove the as-prepared TiO₂/GQD contains COOH functional groups that

will result in a good hydrophilic property and leads to enhanced photocatalysis [38].

The results of the XRD analysis of the synthesized TiO₂/GQD nanocomposite in the (Fig. 11) shows diffraction patterns at 2 25.52°, 48.23°, 38.00° and 55.25 (blue peaks). Moreover, the very weak some peaks of GQD shift to more two

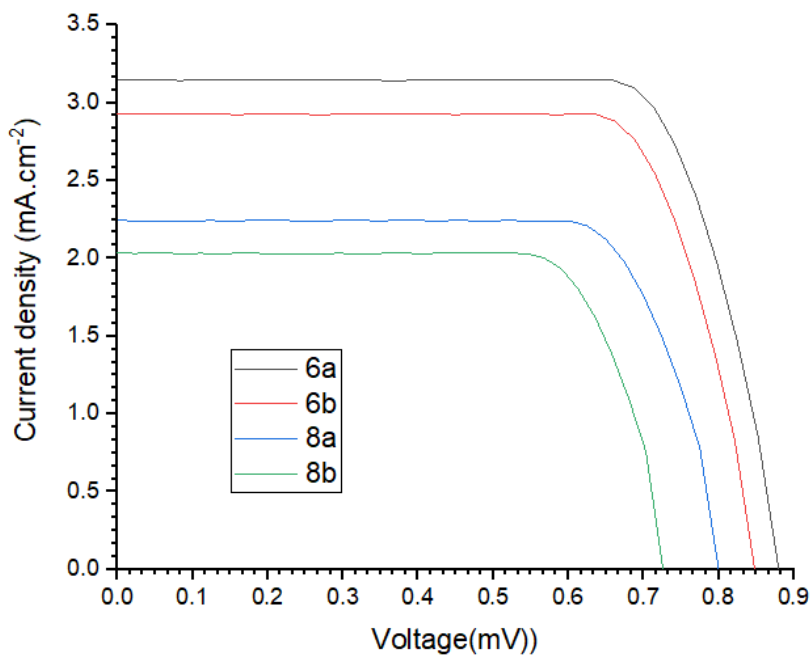


Fig. 12. J-V curve of DSSCs sensitized by 6a,6b,8a and 8b.

Table 2. Photovoltaic characteristics for all colors in a typical environment

Dye	J_{sc} (mA.cm ⁻²)	V_{oc} (mV)	FF (%)	PCE (%)
6a	2.5	0.852	67.6	1.82
6b	2.28	0.821	77.3	1.86
8a	1.60	0.775	77.3	1.34
8b	1.39	0.703	79.7	1.14

theta and be about 29.03° and 22.92° (red peaks). That proved the composite is prepared and TiO₂ is loaded on GQD surface. Using Scherer's equation (1), the mean crystallite size (L) in nm for TiO₂/GQD nano composite was determined to be 38.39 nm. The size of the generated composite seems to be nanomaterial (less than 100 nm)[38, 39].

Dye Sensitized Solar Cells test

The J-V curve was used to compute the open-circuit voltage (V_{oc}) and short circuit current (J_{sc}). The following equations were used to calculate the solar cells' efficiency and fill factor (FF) [40].

$$FF = \frac{J_{max} V_{max}}{J_{sc} V_{oc}} \quad (2)$$

$$\eta = \frac{J_{sc} V_{oc} FF}{I_0} \quad (3)$$

Where I_0 is the total incident irradiance, V_{max} is the solar cell's maximum power point voltage, and J_{max} is the maximum power point current. J_{sc} , V_{oc} , FF, and PCE findings are shown in (Fig. 12) together with the J-V curves for all produced compounds (Table 2). The efficiencies of using compounds 6a and 6b in solar cell are more than the efficiencies of using compounds 8a and 8b. That due to compounds 6a and 6b contain two porphyrin groups that includes six hydroxy groups as an auxochrome.

Form the other hand, compounds 8a is more active than compound 8b because compounds 8a derivatives with imidazole group that give high electric density for Lon pair electron of nitrogen atom.

CONCLUSION

In summary, this work involved the preparation of graphene quantum dots (GQDs) through a hydrothermal method. The GQD was incorporated with TiO₂ by metallic bonds as a nano-composite. Series of porphyrin derivatives were used as sensitizers in solar cells via adsorbing them onto the surface of the GQD/TiO₂ paste. The paste was applied to the FTO surface using Triton X-100 as

a linking material. All the prepared derivatives were found to be sensitive enough to function as solar cells. The most efficient compounds were found to be 6a and 6b, which achieved power conversion efficiencies (PCE) of 1.82% and 1.86%, respectively. Compounds 8a and 8b also showed promising results, with PCEs of 1.34% and 1.14%, respectively, indicating their potential for using in solar cell applications.

ACKNOWLEDGMENTS

The Authors gratefully acknowledge all personnel who support this manuscript in faculty of science and faculty of Engineering the University of Kerbala department of chemistry and department of Petroleum Engineering.

CONFLICT OF INTEREST

The authors declare that there is no conflict of interests regarding the publication of this manuscript.

REFERENCES

1. Ma M, Hu X, Zhang C, Deng C, Wang X. The optimum parameters to synthesize bright and stable graphene quantum dots by hydrothermal method. *Journal of Materials Science: Materials in Electronics*. 2017;28(9):6493-6497.
2. Tang L, Ji R, Cao X, Lin J, Jiang H, Li X, et al. Deep Ultraviolet Photoluminescence of Water-Soluble Self-Passivated Graphene Quantum Dots. *ACS Nano*. 2012;6(6):5102-5110.
3. Chen W, Li D, Tian L, Xiang W, Wang T, Hu W, et al. Synthesis of graphene quantum dots from natural polymer starch for cell imaging. *Green Chem*. 2018;20(19):4438-4442.
4. Zhang M, Bai L, Shang W, Xie W, Ma H, Fu Y, et al. Facile synthesis of water-soluble, highly fluorescent graphene quantum dots as a robust biological label for stem cells. *J Mater Chem*. 2012;22(15):7461.
5. Xu X, Zhou J, Jestin J, Colombo V, Lubineau G. Preparation of water-soluble graphene nanoplatelets and highly conductive films. *Carbon*. 2017;124:133-141.
6. Zhao H, Benetti D, Tong X, Zhang H, Zhou Y, Liu G, et al. Efficient and stable tandem luminescent solar concentrators based on carbon dots and perovskite quantum dots. *Nano Energy*. 2018;50:756-765.
7. Zhao H, Liu G, You S, Camargo FVA, Zavelani-Rossi M, Wang X, et al. Gram-scale synthesis of carbon quantum dots with a large Stokes shift for the fabrication of eco-friendly and high-efficiency luminescent solar concentrators. *Energy and Environmental Science*. 2021;14(1):396-406.
8. Kamat PV. Boosting the Efficiency of Quantum Dot Sensitized

- Solar Cells through Modulation of Interfacial Charge Transfer. *Acc Chem Res.* 2012;45(11):1906-1915.
9. Li Y, Hu Y, Zhao Y, Shi G, Deng L, Hou Y, et al. An Electrochemical Avenue to Green-Luminescent Graphene Quantum Dots as Potential Electron-Acceptors for Photovoltaics. *Adv Mater.* 2010;23(6):776-780.
 10. O'Regan B, Grätzel M. A low-cost, high-efficiency solar cell based on dye-sensitized colloidal TiO₂ films. *Nature.* 1991;353(6346):737-740.
 11. Nazeeruddin MK, Péchy P, Renouard T, Zakeeruddin SM, Humphry-Baker R, Comte P, et al. Engineering of Efficient Panchromatic Sensitizers for Nanocrystalline TiO₂-Based Solar Cells. *Journal of the American Chemical Society.* 2001;123(8):1613-1624.
 12. Saud A, Oves M, Shahadat M, Arshad M, Adnan R, Qureshi MA. Graphene-based organic-inorganic hybrid quantum dots for organic pollutants treatment. *Graphene Quantum Dots: Elsevier;* 2023. p. 133-155.
 13. Kim BG, Zhen CG, Jeong EJ, Kieffer J, Kim J. Organic Dye Design Tools for Efficient Photocurrent Generation in Dye-Sensitized Solar Cells: Exciton Binding Energy and Electron Acceptors. *Adv Funct Mater.* 2012;22(8):1606-1612.
 14. Choi H, Baik C, Kang SO, Ko J, Kang MS, Nazeeruddin MK, et al. Highly Efficient and Thermally Stable Organic Sensitizers for Solvent-Free Dye-Sensitized Solar Cells. *Angew Chem Int Ed.* 2007;47(2):327-330.
 15. Lin RY, Wu FL, Li CT, Chen PY, Ho KC, Lin JT. High-Performance Aqueous/Organic Dye-Sensitized Solar Cells Based on Sensitizers Containing Triethylene Oxide Methyl Ether. *ChemSusChem.* 2015;8(15):2503-2513.
 16. Kim J, Lee B, Kim YJ, Hwang SW. Enhancement of Dye-sensitized Solar Cells Efficiency Using Graphene Quantum Dots as Photoanode. *Bull Korean Chem Soc.* 2018;40(1):56-61.
 17. Wei Y, Chen Y, Yuan R, Xue Z, Zhao L. Substitution effects of zinc porphyrin-sensitized TiO₂ nanoparticles for photodegradation of AB1. *J Mol Struct.* 2023;1277:134889.
 18. Zamiri G, Bagheri S. Fabrication of green dye-sensitized solar cell based on ZnO nanoparticles as a photoanode and graphene quantum dots as a photo-sensitizer. *Journal of Colloid and Interface Science.* 2018;511:318-324.
 19. Min Park J, Lee JH, Jang W-D. Applications of porphyrins in emerging energy conversion technologies. *Coord Chem Rev.* 2020;407:213157.
 20. Ghosh NN, Saha S, Pramanik A, Sarkar P, Pal S. Molecular design of porphyrin dyes using different electron-withdrawing moieties for high performance dye-sensitized solar cells. *Computational and Theoretical Chemistry.* 2020;1182:112846.
 21. Verma S, Ghosh A, Das A, Ghosh HN. Exciton-Coupled Charge-Transfer Dynamics in a Porphyrin J-Aggregate/TiO₂ Complex. *Chemistry – A European Journal.* 2011;17(12):3458-3464.
 22. Shi X, Chen R, Jiang T, Ma S, Liu X, Ding Y, et al. Regulation of Interfacial Charge Transfer and Recombination for Efficient Planar Perovskite Solar Cells. *Solar RRL.* 2019;4(2).
 23. Chen Y, Huang R, Chen D, Wang Y, Liu W, Li X, et al. Exploring the Different Photocatalytic Performance for Dye Degradations over Hexagonal ZnIn₂S₄ Microspheres and Cubic ZnIn₂S₄ Nanoparticles. *ACS Applied Materials and Interfaces.* 2012;4(4):2273-2279.
 24. Chen Y, Mo Z, Zhu X, Xu Q, Xue Z, Li H, et al. Facilitated interfacial charge separation using triphenylamine-zinc porphyrin dyad-sensitized TiO₂ nanoparticles for photocatalysis. *J Alloys Compd.* 2021;889:161795.
 25. Ahmed LM, Ivanova I, Hussein FH, Bahnmann DW. Role of Platinum Deposited on TiO₂ in Photocatalytic Methanol Oxidation and Dehydrogenation Reactions. *International Journal of Photoenergy.* 2014;2014:1-9.
 26. Jassim S, Abbas A, Al-Shakban M, Ahmed L. Chemical Vapour Deposition of CdS Thin Films at Low Temperatures from Cadmium Ethyl Xanthate. *Egyptian Journal of Chemistry.* 2021;64(5):3-4.
 27. Obeidat A, Alqaiem S, Al-Qawasmeh A, Badarneh M, Qaseer M-K. Magnetic and Thermodynamic Properties of a Copper Fluorides (Inverse Spinel-Like Structure: A Monte Carlo Study. *SSRN Electronic Journal.* 2022.
 28. Ahmed L, Alkhafaji E, Oda N. Characterization of silver nanohybrid with layers double hydroxide and demonstration inhibition of antibiotic-resistance *Staphylococcus aureus.* *Egyptian Journal of Chemistry.* 2022;0(0):0-0.
 29. Oosawa Y. Photocatalytic hydrogen evolution from an aqueous methanol solution over ceramics-electrocatalyst/TiO₂. *Chem Lett.* 1983;12(4):577-580.
 30. Abed z, Mohammad R, Eltayef A. Structural properties of Ag-CuO thin films on silicon prepared via DC magnetron sputtering. *Egyptian Journal of Chemistry.* 2021;0(0):0-0.
 31. Ahmed L, Ali S, Ali M. Hybrid Phosphotungstic acid -Dopamine (PTA-DA) Like-flower Nanostructure Synthesis as a Furosemide Drug Delivery System and Kinetic Study of Drug Releasing. *Egyptian Journal of Chemistry.* 2021;0(0):0-0.
 32. Ali SMH, Alali MMMA, Ahmed LM. Flower-like hierarchical nanostructures synthesis of polyoxometalate-dopamine and loading furosemide on its surface and aging them using microwave technique. The 9th international conference on applied science and technology (ICAST 2021): AIP Publishing; 2022.
 33. Obaid A, Ahmed L. One-Step Hydrothermal Synthesis of α-MoO₃ Nano-belts with Ultrasonic Assist for incorporating TiO₂ as a NanoComposite. *Egyptian Journal of Chemistry.* 2021;0(0):0-0.
 34. Ghosh D, Biswas R. Theoretical Calculation of Absolute Radii of Atoms and Ions. Part 2. The Ionic Radii. *Int J Mol Sci.* 2003;4(6):379-407.
 35. Halbus AF, Hussein FH. Photocatalytic Decolorization of Cobalamin in Aqueous Suspensions of TiO₂ and ZnO Under Solar Irradiation. *Asian J Chem.* 2014;26(4):1207-1211.
 36. Ahmed L, Kadhim H, Al-Hachamii M. Facile Synthesis of Spinel CoCr₂O₄ and Its Nanocomposite with ZrO₂: Employing in Photo-catalytic Decolorization of Fe (II)-(luminol-Tyrosine) Complex. *Egyptian Journal of Chemistry.* 2021;0(0):0-0.
 37. Hassan SS, Zehra SS, Ahmed Z, Talpur MYY, Panhwar S. Removal of arsenic contaminants from water using iron oxide nanoparticles by inductively coupled plasma mass spectrometry. *Research Square Platform LLC;* 2022.
 38. Ridha NJ, Mohamad Alosfur FK, Kadhim HBA, Ahmed LM. Synthesis of Ag decorated TiO₂ nanoneedles for photocatalytic degradation of methylene blue dye. *Materials Research Express.* 2021;8(12):125013.
 39. Raees A, Jamal M, Ahmed I, Silanpaa M, Saad Algarni T. Synthesis and Characterization of CeO₂/CuO Nanocomposites for Photocatalytic Degradation of Methylene Blue in Visible Light. *Coatings.* 2021;11(3):305.
 40. Umale S, Sudhakar V, Sontakke SM, Krishnamoorthy K, Pandit AB. Improved efficiency of DSSC using combustion synthesized TiO₂. *Mater Res Bull.* 2019;109:222-226.